Robotica (2009) volume 27, pp. 355–365. © 2008 Cambridge University Press
doi:10.1017/S026357470800475X Printed in the United Kingdom

Genetic algorithm-based optimal bipedal walking gait synthesis considering tradeoff between stability margin and speed

Goswami Dip, Vadakkepat Prahlad* and Phung Duc Kien

Department of Electrical and Computer Engineering, National University of Singapore, 4 Engineering Drive 3, Singapore 117576.

(Received in Final Form: May 5, 2008. First published online: June 18, 2008)

SUMMARY

The inverse kinematics of a 12 degrees-of-freedom (DOFs) biped robot is formulated in terms of certain parameters. The biped walking gaits are developed using the parameters. The walking gaits are optimized using genetic algorithm (GA). The optimization is carried out considering relative importance of stability margin and walking speed. The stability margin depends on the position of zero-moment-point (ZMP) while walking speed varies with step-size. The ZMP is computed by an approximation-based method which does not require system dynamics. The optimal walking gaits are experimentally realized on a biped robot.

KEYWORDS: Biped robot; Inverse kinematics; Zero-moment-point; Stability margin; Walking speed; Genetic algorithm.

1. Introduction

Gait generation for bipedal systems is being studied for more than two decades. Gait generation involves major research directions such as actuator-level trajectory generation using simplified bipedal models, joint trajectory generation based on postural stability analysis, biologically inspired approaches to generate gait, and learning and optimization of bipedal gaits.

Dynamics of biped systems is nonlinear and difficult to analyze.[1] In certain studies simplified biped models are utilized. The most popular and widely used model is the inverted pendulum model.[2–4,10] In this model the whole body is replaced with a concentrated mass located at the center-of-mass (CM). Bio-mechanical concepts and inverted pendulum models are often utilized to generate walking gaits for simplified two-legged mechanisms.[25,26] Inverted pendulum model is useful for stability analysis of bipeds by computing the zero-moment-point (ZMP) which is the point on the ground where the resultant of every moment is zero.[4] Combining 1-degree-of-freedom (DOF) inverted pendulum model for stance leg and 2-DOF inverted pendulum model for swing leg simplifies walking gait generation.[2] Self-excitation control of inverted pendulum model leads to passive dynamic walking.[3] A running-cart-table model simplifies the estimation of variation in ZMP during bipedal activities.[7]

* Corresponding author. E-mail: prahlad@ieee.org

Postural stability of legged systems is analyzed by the concept of ZMP introduced by Vukobratović *et al.* in early nineties.[1] The postural stability of legged systems is ensured by keeping the ZMP within the area covered by foot, i.e., the support polygon. The most common approach for gait generation is to compute trajectories maintaining postural stability using system dynamics.[5,7,9] Decoupling the subsystems reduces the complexity in bipedal gait generation.[6] Decoupled and linearized dynamic equations simplify the ZMP computation.[5] Injection of torque at the ankle provides ZMP compensation to maintain postural stability during various bipedal activities.[8] By maintaining the CM at a specific height, the linear inverted pendulum model generates stable walking gait.[9] ZMP-based gait generation is utilized by the ASIMO humanoid.[20]

Biologically inspired approaches generate natural walking gaits[27–30] in particular biped gaits.[11,12,21,22] Neural oscillators are suitable for learning stable walking patterns on unknown surface conditions.[11] Genetic algorithm (GA) is an effective tool to optimize neural oscillators generating natural walking patterns.[12] In biological systems, central pattern generators (CPG) produce the basic rhythmic leg movements as well as leg coordination.[23,24] Biological locomotion mostly relies on CPG and sensory feedback (reflexive mechanism).[23,24] The concept of CPG is realized using adaptive neural oscillators in ref. [21]. Human-like reflexive-mechanisms are often used for learning walking gaits.[22]

1.1. Related works

Several techniques exist to learn and optimize bipedal gaits based on objectives such as minimizing energy consumption and maximizing stability margin, speed, and learning rate. Neural Network (NN)[10–12,22,23] reinforcement learning (RL),[11,31] imitation-based approaches,[13] and GA[12,19] are the learning and optimization tools used in bipedal gait synthesis.

NN is a widely used technique for gait generation. Unsupervised and supervised learning methods are adopted in training NN. RL (unsupervised) and human motion capture data and GA (supervised) are tools useful to train NN for bipedal gait generation. In the unsupervised approach the learning process is dependent on the feedbacks from the training environment.[22] Supervised training of NN requires large number of training data for generalization.

RL relies on sensory feedback from the environment.[11,31] The associated learning process should utilize enough

training data to enhance the generalization capabilities of the learned gaits, which is a tedious task. It is desirable to utilize the kinematic and dynamic models for faster dynamic walking.

Visual information of human locomotion or motion capture data are often used in biped locomotion to imitate human walking gait.[13] Performance of the imitation-based approaches depends on the vision systems used for capturing motion data. They are difficult to experimentally realize due to lack of dynamical analysis and hardware restrictions.

GA is a powerful tool to resolve the issues related to the optimality of biped gaits. The major application of GA is in optimal training of NN.[12,19] GA is utilized for bipedal gait generation by minimizing a weighted cost function of the input energy and ZMP error generating training data set for a three-layer NN in ref. [19]. The effects of hardware and mechanical constraints are not clearly brought out due to lack of experimental validation. The impact of variations in parameters and walking speed on dynamic stability is also not addressed.

Apart from the optimal training of NN, GA is useful for other purposes in bipedal locomotion. GA-based path planning produces smooth bipedal movements.[14,19] GA-optimized *computed-torque* control architecture improves actuator-level control.[15] GA-optimized spline trajectories result in bipedal gaits with minimal energy consumption.[17]

In this work, GA is utilized to optimize the gait parameters in solving the inverse kinematics model. The walking gaits are generated based on the optimal parameters. The description of the biped, actuators, and the mechanical design are provided in Section 2. Inverse kinematics is formulated for a 12-DOF biped robot in terms of certain gait parameters. Inverse kinematic model and walking gait generation are described, respectively, in Sections 3 and 4. The walking gaits are optimized using GA considering relative importance between stability margin and speed of walking. Section 5 discusses the GA-based gait optimization. The ZMP computation method for gait optimization is outlined in Section 6. The optimized walking gait is experimentally realized on a biped robot. The tradeoff between walking speed and stability margin are brought out. With increase in speed, walking becomes dynamic (less stable) and vice versa. The experimental results are discussed in Section 7, while the paper concludes in Section 8.

2. Biped Model, Actuators, and Mechanical Design

The biped robot consists of two legs. The waist-link connects the two legs. Each leg has three links: foot-link, shank-link, and thigh-link. The joint between the foot-link and shank-link is the ankle, the joint between shank-link and thigh-link is the knee while the one between thigh-link and waist-link is the hip. The biped has 12 DOFs. Two DOFs at ankle, 1 DOF at knee, and 3 DOFs at hip, i.e., 6 DOFs in each leg (Fig. 1). Each DOF corresponds to an independent actuator.

The links are made of light-weight aluminium which leads to their little contribution to the overall mass or inertia of the link. The overall mass or inertia of the links are computed based on the positions and weights of the actuators which are located at the joints between two links. The link masses

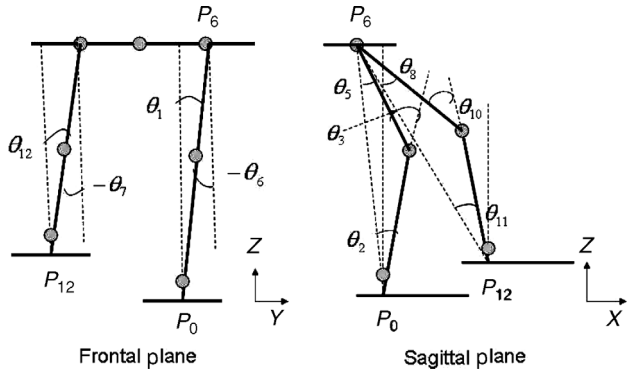

Fig. 1. Generalized coordinates.

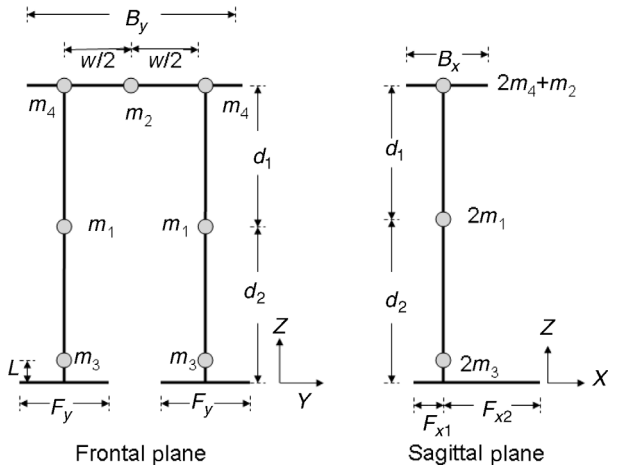

Fig. 2. Biped model: mass distribution.

are assumed concentrated at the joints located at the distal ends. The mass distribution of the biped is shown in Fig. 2. ‘‘d_1” indicates the thigh-link length and “d_2” the shank-link length. “F_y” and “F_x” are the foot width and length. “F_{x1}” and “F_{x2}” are the distances from the ankle to the rear and front edges of the foot. “B_y” and “B_x” are the hip-link width and length. The distance between two hip-joints is “w”, and the distance between the ankle-joint and CM of the foot is “L”. Table I provides the parameter values.

Table I. Parameters of the robot.

Parameters	Values
m_1	0.07 kg
m_2	0.02 kg
m_3	0.14 kg
m_4	0.21 kg
d_1	0.19 m
d_2	0.15 m
w	0.12 m
L	0.02 m
B_x	0.1 m
B_y	0.14 m
F_{x1}	0.03 m
F_{x2}	0.07 m
F_y	0.055 m

https://doi.org/10.1017/S026357470800475X Published online by Cambridge University Press

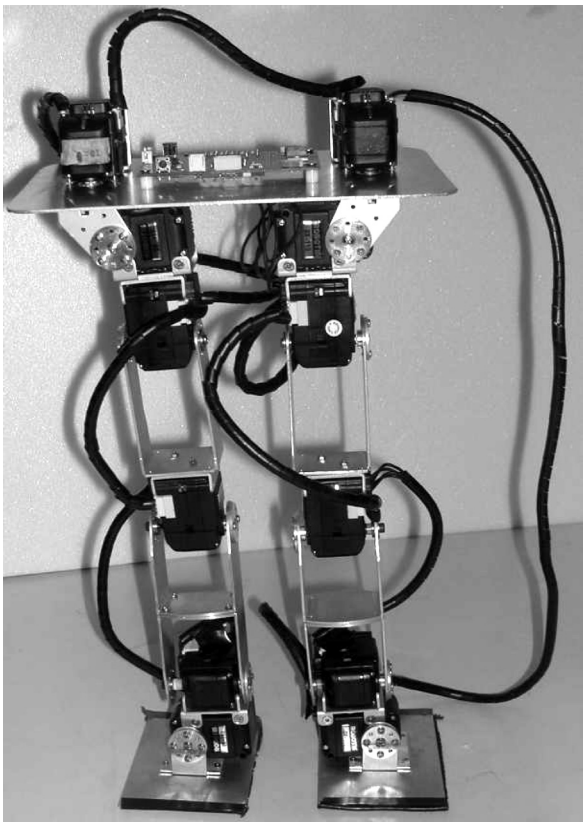

Fig. 3. The biped.

Dynamixel motors (DX-113) from Robotis Inc. (www.tribotix.com) are used as actuators. The motors are compact and light-weight (58 g) providing high torque (a maximum holding torque of 1.02 Nm). The motors have a control-network with position and velocity feedbacks. Each motor along with associated mechanical components weighs around 70 g which is reflected in Table I. The control instructions are sent to the motors from MATLAB environment by RS-485 serial communication. The mechanical structure of the biped is shown in Fig. 3.

3. Biped Inverse Kinematics

3.1. Generalized coordinates

The biped has 12 DOFs realized by 12 actuators placed at the joints. Any specific configuration of the biped is expressed by a 12×1 vector of generalized coordinates, $[\theta_1, \theta_2, \ldots, \theta_{12}]^T$, as shown in Fig. 1.

3.2. Inverse kinematics

The Cartesian coordinates of the reference points $P_i(P_{ix}, P_{iy}, P_{iz})$ are shown in Fig. 4. $P_{0,12}$ are the ankle joints, $P_{3,10}$ are the knee joints, and P_6 is the hip joint. $P_{0,3,6}$ are joints of the stance leg and $P_{10,12}$ are the joints of the swing leg. Positions of the motors are such that the CM of the foot-links does not coincide with the ankle-joints. The point P_{0m} is the Cartesian coordinate of the CM of the stance leg foot-link while P_{12m} is that of the swing leg foot-link.

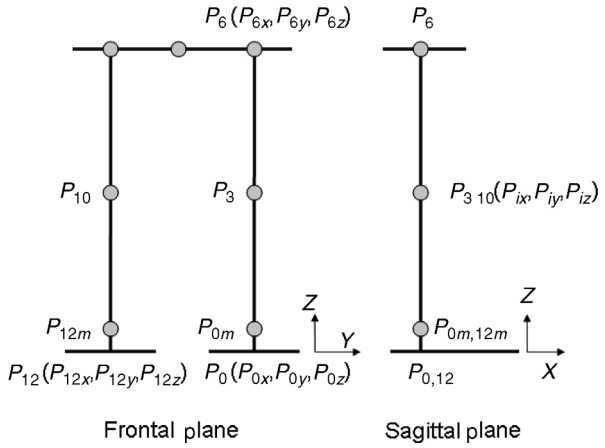

Fig. 4. Biped reference points for inverse kinematics.

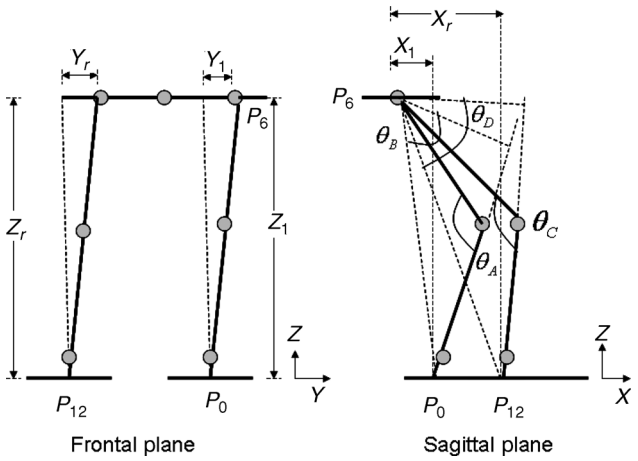

Fig. 5. Biped: inverse kinematic parameters.

The inverse kinematic parameters are defined as (Fig. 5)

$$x_1 = P_{0x} - P_{6x}, y_1 = -P_{6y}, z_1 = P_{0z} - P_{6z},$$
$$x_r = P_{12x} - P_{6x}, y_r = -P_{6y}, z_r = P_{12z} - P_{6z}. \quad (1)$$

x_1 and x_r are the displacements of the hip along sagittal plane with respect to the corresponding ankle. y_1 and y_r are the displacements of the hip along frontal plane with respect to the corresponding ankle. z_1 and z_r are the heights of the hip from the ankle. Four angular quantities (Fig. 5) are defined as per (2).

$$\theta_A = \cos^{-1}\left[\frac{d_1^2 + d_2^2 - x_1^2 - y_1^2 - z_1^2}{2d_1 d_2}\right]$$
$$\theta_B = \cos^{-1}\left[\frac{d_1 \sin(\theta_A)}{\sqrt{x_1^2 + y_1^2 + z_1^2}}\right]$$
$$\theta_C = \cos^{-1}\left[\frac{d_1^2 + d_2^2 - x_r^2 - y_r^2 - z_r^2}{2d_1 d_2}\right]$$
$$\theta_D = \cos^{-1}\left[\frac{d_1 \sin(\theta_C)}{\sqrt{x_r^2 + y_r^2 + z_r^2}}\right]. \quad (2)$$

https://doi.org/10.1017/S026357470800475X Published online by Cambridge University Press

The expressions for the generalized coordinates in terms of the inverse kinematic parameters are provided in (3). For straight walking, $y_1 = y_r$ and $\theta_4 = \theta_9 = 0$.

$$\begin{aligned}
\theta_1 &= \tan^{-1}\left(\frac{y_1}{z_1}\right),\\
\theta_{12} &= \tan^{-1}\left(\frac{y_r}{z_r}\right),\\
\theta_6 &= -\theta_1,\\
\theta_7 &= -\theta_{12},\\
\theta_3 &= \pi - \theta_A,\\
\theta_{10} &= \pi - \theta_C,\\
\theta_5 &= \frac{\pi}{2} - \theta_A + \theta_B + \sin^{-1}\left(\frac{x_1}{\sqrt{x_1^2 + y_1^2 + z_1^2}}\right),\\
\theta_8 &= \frac{\pi}{2} - \theta_C + \theta_D + \sin^{-1}\left(\frac{x_r}{\sqrt{x_r^2 + y_r^2 + z_r^2}}\right),\\
\theta_4 &= 0,\\
\theta_9 &= 0,\\
\theta_2 &= \theta_3 - \theta_5,\\
\theta_{11} &= \theta_{10} - \theta_8. \qquad (3)
\end{aligned}$$

4. Biped Walking Gait

The walking gait is expressed in terms of the following parameters: step-length s, bending-height h, maximum lifting-height H, maximum frontal-shift n, and step-time T (Fig. 6). During walking, the height of the waist-link is kept constant.

The biped walking motion is generated by choosing an appropriate time function for the three reference points: $P_0(P_{0x}, P_{0y}, P_{0z})$, $P_6(P_{6x}, P_{6y}, P_{6z})$, and $P_{12}(P_{12x}, P_{12y}, P_{12z})$. P_0 is stationary for $0 \le t \le T$ and acts as a reference for P_6 and P_{12}. For $T < t \le 2T$, the positions of P_0 and P_{12} are interchanged. P_0, P_6, and P_{12} are chosen intuitively. P_0 and P_{12} are selected according to the desired leg movement for a specific activity. The choice of P_6 depends on the mechanical structure of the biped as it involves shifting of ZMP from one foot to another. In a walking cycle, $0 \le t \le 2T$, P_0 and P_{12} for straight walking are provided by (4).

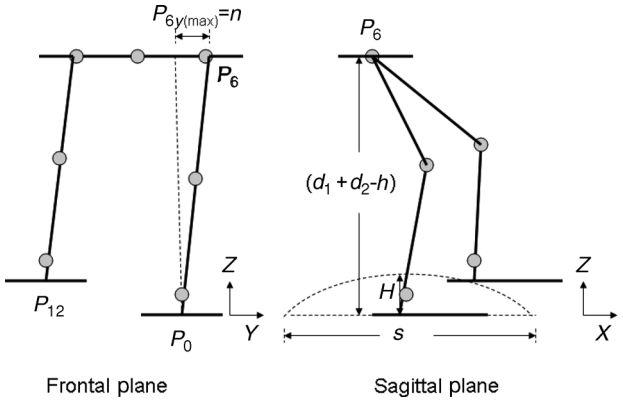

Fig. 6. Gait generation parameters.

$$\begin{aligned}
P_{0x}(t) &= \left(\frac{s}{2}\right)\sin\left(\frac{\pi}{T}\left(t - \frac{T}{2}\right)\right)(u(t-2T) - u(t-T)),\\
P_{0y}(t) &= -w(u(t-2T) - u(t-T)),\\
P_{0z}(t) &= H\sin\left(\pi\left(\frac{P_{0x}(t)}{s} + 0.5\right)\right)(u(t-2T) - u(t-T)),\\
P_{12x}(t) &= \left(\frac{s}{2}\right)\sin\left(\frac{\pi}{T}\left(t - \frac{T}{2}\right)\right)(u(t) - u(t-T)),\\
P_{12y}(t) &= -w(u(t) - u(t-T)),\\
P_{12z}(t) &= H\sin\left(\pi\left(\frac{P_{12x}(t)}{s} + 0.5\right)\right)(u(t) - u(t-T)), \qquad (4)
\end{aligned}$$

where $u(.)$ is a unit step function given by (5).

$$u(t) = \begin{cases} 1 & \text{if } t \ge 0,\\ 0 & \text{otherwise.} \end{cases} \qquad (5)$$

P_6 for straight walking is given by (6).

$$\begin{aligned}
P_{6x}(t) &= \left(\frac{s}{4}\right)\sin\left(\frac{\pi}{T}\left(\tau - \frac{T}{2}\right)\right),\\
P_{6y}(t) &= n\sin\left(\frac{\pi}{2}\left(\sin\left(\frac{\tau\pi}{2T}\right) + 1\right)\right)\sin\left(\pi\frac{t}{T}\right),\\
P_{6z}(t) &= (d_1 + d_2 - h), \qquad (6)
\end{aligned}$$

where for $0 \le t \le T$, $\tau = t$ and for $T \le t \le 2T$, $\tau = t - T$. When P_0, P_6, and P_{12} are as per (4) and (6), the biped robot walks straight. The walking gait is generated by sampling the functions in (4) and (6) at certain intervals. In (4) and (6), t and T govern the sampling process which decides the walking speed and the smoothness of the walking gaits. With Δt as the sampling interval, $(\frac{T}{\Delta t})$ indicates the number of samples in T seconds or sampling frequency. A too low $(\frac{T}{\Delta t})$ results in mechanical jerking during walking which can lead to erratic movement and instability. A too high $(\frac{T}{\Delta t})$ causes computational burden on the hardware making the walking process very slow. For a given system, the values of T and Δt should be chosen accordingly. There can be various combinations of walking parameters, i.e., s, h, H, and n that generate straight walking gaits. Selection of optimal walking parameters is discussed in Section 5.

5. GA-Based Parameter Optimization

This section discusses the selection of the parameters s, h, H, and n for straight walking, considering the step-time T as unity. The values of the parameters are computed considering a tradeoff between stability and speed of walking.

https://doi.org/10.1017/S026357470800475X Published online by Cambridge University Press

5.1. Constrains on walking parameters

Mechanical design of the biped robot brings constrains on the maximum and minimum ranges of feasible values of the walking parameters. Following are the constrains on the walking parameters which are arrived at experimentally:

$$\begin{aligned} 0.05 \leq s &\leq 0.13, \\ 0.001 \leq n &\leq 0.13, \\ 0.001 \leq H &\leq 0.13, \\ 0.001 \leq h &\leq 0.13. \end{aligned} \tag{7}$$

5.2. Postural stability considering ZMP

For legged systems with foot, the ZMP should fall inside the support polygon for postural stability. In double-support walking phase the feet are in contact with the ground, while only the stance leg is in contact with the ground in single-support phase. During single-support phase, the area of the support polygon is same as the area covered by the stance leg foot.

For the biped model considered, let the Cartesian coordinate of the ZMP be $(x_{\text{zmp}}, y_{\text{zmp}}, 0)$. During single-support phase, the conditions for postural stability of the biped are

$$\begin{aligned} -F_{x1} \leq x_{\text{zmp}} &\leq F_{x2}, \\ -\frac{F_y}{2} \leq y_{\text{zmp}} &\leq \frac{F_y}{2}. \end{aligned} \tag{8}$$

Walking is static if the conditions in (8) are satisfied during the entire walking cycle. During dynamic walking, the conditions are not met for the entire walking cycle.

5.3. Cost function

Stability of biped systems is quantified by the distance of its ZMP from the stance foot ankle-joint during single-support phase. The walking gait with maximum stability margin is obtained by minimizing (9).

$$Q = \int_0^T \left(x_{\text{zmp}}^2 + y_{\text{zmp}}^2\right) \mathrm{d}t. \tag{9}$$

The walking parameters corresponding to the minimum value of Q generate gaits with maximum stability margin. When walking speed is factored in the optimization process, the step-length (s) appears in the cost function. Let us define functions

$$\begin{aligned} f_1 &= \frac{1}{Q}, \\ f_2 &= s. \end{aligned} \tag{10}$$

Let the maximum numerical values of f_1 and f_2 are $f_1^{\max}$ and $f_2^{\max}$, respectively. The expression for the normalized cost function is given in (11).

$$f = \frac{\lambda f_1}{f_1^{\max}} + \frac{(1-\lambda) f_2}{f_2^{\max}}, \tag{11}$$

where $0 \leq \lambda \leq 1$. The cost function (11) has maximum value with either $\lambda = 1.0$ or $\lambda = 0$. λ is not used as a parameter in the GA-based optimization, rather it is left unchanged during the optimization process. The optimal walking gait parameters are obtained maximizing the cost function (11) for a specific value of λ. The walking parameters corresponding to $\lambda = 1$ generate the most stable gait. Speed of walking is maximum when $\lambda = 0$. Intuitively, when the step-length *"s"* is smaller, stability margin is higher. Small step-length *"s"* produces slow walking. GA is utilized to obtain the optimal walking parameters by maximizing the cost function (11) after selecting λ as a tradeoff between the walking speed and stability margin.

Table II. Parameters of GA.

Parameters	Values
Chromosome size	4
Population size	30
No. of epoch	30
Mutation rate	0.1
Crossover rate	0.8

5.4. Genetic algorithm

GA, with parameters in Table II, is utilized to optimize the walking parameters by maximizing the cost function (11). The block diagram of the GA algorithm is shown in Fig. 7. Floating point strings are used and the initial *population* is chosen randomly satisfying the constrains in (7). *Single-point crossover* is performed by swapping the values of two

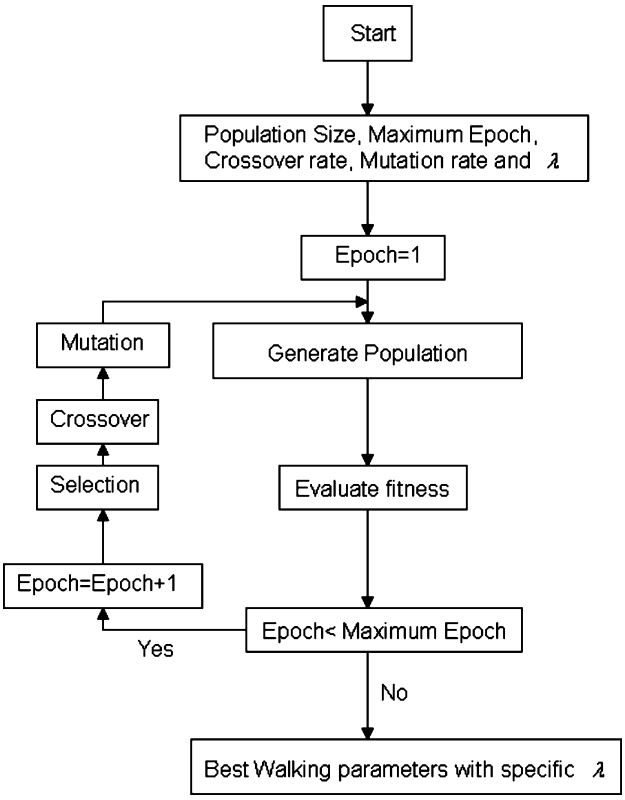

Fig. 7. The GA algorithm for obtaining optimal walking parameters for a specific value of λ.

https://doi.org/10.1017/S026357470800475X Published online by Cambridge University Press

chromosomes after *tournament selection*. *Mutation* is carried out by flipping the values of *alleles*. For example,

Before mutation: $0.05 \leq s = 0.07 \leq 0.13$
After mutation: $s = (0.05 + 0.13) - 0.07.$

Using GA, the optimal walking parameters are obtained for different λ.

In the GA-based gait generation approach, the following points are noticeable:

- Various kinds of bipedal locomotion (for example, stair climbing and obstacle avoiding) can be generated using inverse kinematics (3). However, the expressions for P_0, P_6, and P_{12} in (4) and (6) will change for different activities. Depending on the size (height) of the obstacle (stair), the values of parameters s, h, H, and n will change requiring redoing the optimization.
- Bipedal gaits to follow curvilinear paths are generated by choosing appropriate expressions for θ_4 and θ_9 in (3). For example, $\theta_9 = K$, a positive constant for $0 \leq t \leq T$ and $\theta_4 = K$ for $T < t \leq 2T$ makes the robot move in a circular path. Due to mechanical constraints and walking stability, $K \leq 8^0$ and $\lambda \geq 0.7$ are maintained.

6. Computation of ZMP

To compute the cost function (11), the ZMP positions are required at every integration step. Conventional methods[1] of computing ZMP involve computation of system dynamics which is tedious and requires high computational effort. An approximation-based approach of ZMP computation is used in this work which does not require system dynamics.

CM, $(x_{\text{cm}}, y_{\text{cm}}, z_{\text{cm}})$, of the biped robot is given by

$$x_{\text{cm}} = \frac{\sum_i m_i P_{ix}}{\sum_i m_i},$$
$$y_{\text{cm}} = \frac{\sum_i m_i P_{iy}}{\sum_i m_i},$$
$$z_{\text{cm}} = \frac{\sum_i m_i P_{iz}}{\sum_i m_i}. \tag{12}$$

The ZMP, $(x_{\text{zmp}}, y_{\text{zmp}}, 0)$, is related to CM by

$$x_{\text{zmp}} = x_{\text{cm}} + \frac{\sum_i m_i P_{ix} \ddot{P}_{iz} - \sum_i m_i P_{iz} \ddot{P}_{ix}}{g \sum_i m_i} + \frac{\sum_i M_{iy}}{g \sum_i m_i},$$
$$y_{\text{zmp}} = y_{\text{cm}} + \frac{\sum_i m_i P_{iy} \ddot{P}_{iz} - \sum_i m_i P_{iz} \ddot{P}_{iy}}{g \sum_i m_i} - \frac{\sum_i M_{ix}}{g \sum_i m_i}, \tag{13}$$

where M_{ix} and M_{iy} are the moments of the links due to rotation about x- and y-axes, respectively. The moments can be computed from the system dynamic equations using Newton–Euler dynamic formulation.[18] In the biped model described in Section 2, the masses are concentrated at the link ends making the inertia tensor of the links zero. Due to zero inertia tensor, the moments, M_{ix} and M_{iy}, are zero.[18] ZMP is computed by

$$x_{\text{zmp}} = x_{\text{cm}} + \frac{\sum_i m_i P_{ix} \ddot{P}_{iz} - \sum_i m_i P_{iz} \ddot{P}_{ix}}{g \sum_i m_i},$$
$$y_{\text{zmp}} = y_{\text{cm}} + \frac{\sum_i m_i P_{iy} \ddot{P}_{iz} - \sum_i m_i P_{iz} \ddot{P}_{iy}}{g \sum_i m_i}. \tag{14}$$

Using (4), (6), and (14), it is possible to determine the closed-form expressions of ZMP which are provided in the appendix.

Link masses are approximately 5–10% of the actuator masses. Height of hip-link being kept unchanged during walking, the robot has nominal rotational movements. Numerical values of M_{ix} and M_{iy} are negligible even when links have distributed mass (which is not the case in this biped model). However, the third terms in (13) might not be negligible for fast bipedal activities like running and jumping, or when the link masses and dimensions are comparable to those of the actuators leading to the necessity to compute system dynamics.

7. Simulations and Experiments

The ZMP expressions are obtained in MATLAB/Simulink environment. These expressions are converted into C language code by using "ccode" command for faster computation and simulation. Runga-Kutta fourth-order method of numerical integration, with fixed time step of 0.0001 s, is used for GA-based optimization. The optimal walking parameters are computed in Microsoft VC++ environment using the generated C code.

The optimal walking parameters are further used in MATLAB environment to compute inverse kinematic solutions for the biped to walk straight and to generate the control instructions for the motors. These instructions are sent to the motors using RS-485 serial communication protocol making the biped walk straight. As the DX-113 motors are capable of communicating with MATLAB, inverse kinematic is solved online and the instructions are sent to the motors.

For computing the cost function f in (11), $f_1^{\max}$ and $f_2^{\max}$ are required. $f_1^{\max}$ is 442.522 corresponding to the maximum value of cost function f_1. $f_2^{\max}$ is obtained from (7) and is equal to 0.13.

Several simulations were run to compute the optimal walking parameters for different values of λ (Table III). Walking becomes slower with higher stability margin. Parameters corresponding to $\lambda = 1$ produce gaits with highest stability margin. Experimentally, it is seen that the biped falls down while trying to walk with parameters for $\lambda < 0.1$. Table III shows the optimum walking parameters for different λ varying from 0.1 to 1.0. Dynamics walking is observed for $\lambda < 0.2$. Walking gaits are realized for λ evenly varying from 0.1 to 0.2. $\lambda = 0.15$ provides satisfactory walking performance on cemented surface. Figure 8 shows the fitness trend in GA-based optimization which converges within 15 epoches. Integration time step for evaluating f

https://doi.org/10.1017/S026357470800475X Published online by Cambridge University Press

Table III. Optimum walking parameters obtained through GA optimization.

λ	s	n	H	h	f
0.10	0.125	0.128	0.010	0.022	0.944
0.15	0.130	0.109	0.014	0.020	0.965
0.20	0.124	0.130	0.006	0.017	0.926
0.40	0.119	0.108	0.018	0.016	0.903
0.60	0.104	0.112	0.013	0.016	0.857
0.90	0.057	0.127	0.017	0.018	0.939
1.0	0.055	0.120	0.026	0.010	1.000

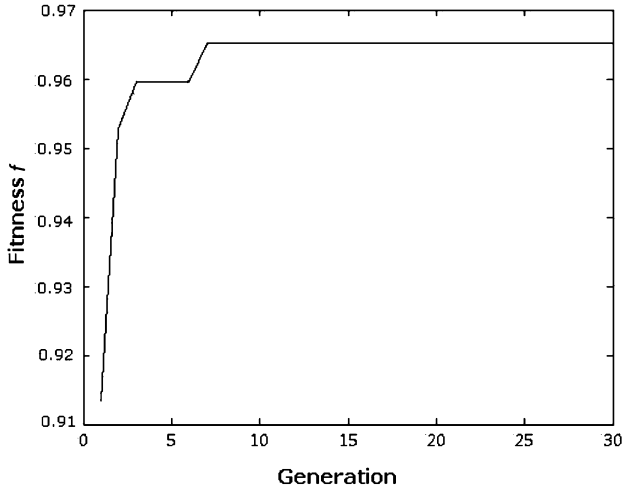

Fig. 8. Fitness trend with $\lambda = 0.15$.

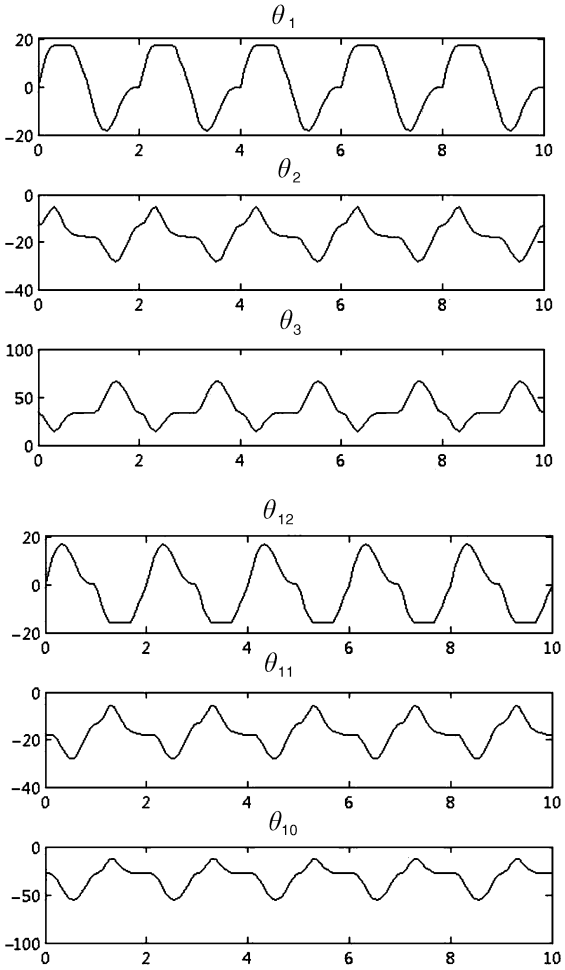

Fig. 9. The walking gait with $\lambda = 0.15$: $\theta_1, \theta_{12}, \theta_2, \theta_{11}, \theta_3, \theta_{10}$ (time in second vs. angle in degree).

in the optimization process is 0.0001 s and one generation corresponds to 300, 000 time steps. Step-time T is 1 s and Δt is 0.1 s. In an Intel Pentium IV processor, the overall optimization process takes approximately 10 min.

As the inverse kinematic is solved at every sampling instant and the communication between MATLAB and the motors has some time delay, the time for one step of walking is more than the step-time T (approximately 1.2 s). The biped's walking gait with $\lambda = 0.15$ is shown in Figs. 9 and 10 for 10 step-times. The biped walking experiment is shown in Fig. 11. The walking speed is about 0.125 m/s.

The variation of ZMP for single step-time of walking cycle with $\lambda = 0.15$ is shown in Figs. 12 and 13. The shaded portions in the figures indicate the single-support phase. The single-support phase is sensed by the current-intake-feedback from the motors. For postural stability of the biped in single-support phase, the ZMP should be within the following ranges (from (8)): $-0.03 \leq x_{\text{zmp}} \leq 0.07$ and $-0.0275 \leq y_{\text{zmp}} \leq 0.0275$. In Figs. 12 and 13, it is seen that the above conditions are not satisfied in certain phases of walking cycle. Therefore, dynamic walking is generated with $\lambda = 0.15$.

7.1. Effect of λ on walking performance

During biped walking (static or dynamic) the duration when the biped is not statically stable decides the stability margin. Stability margin varies with λ. With increase in λ the stability margin increases and vice versa. Stable walking on different surface conditions requires different stability margins. For example, while walking on cemented surface $\lambda = 0.15$ provides satisfactory walking performance. $\lambda = 0.2$ is required for satisfactory walking performance on plywood surface. $\lambda = 0.9$ provides stable walking parameters when wires of thickness 3 mm are placed on the walking surface. The value of λ can be adjusted for stable walking depending on the surface condition or disturbances.

The stability margin is maximum with parameters for $\lambda = 1.0$. Figures 14 and 15 show the variation of ZMP for one step-time when walking on cemented surface. The ZMP positions meet the conditions for static stability (8) for the entire walking cycle. Parameters corresponding to $\lambda = 1$ produce static walking. The static walking speed is approximately 0.05 m/s.

Figures 16 and 17 show the variation of ZMP for one step-time when walking on cemented surface with $\lambda = 0.1$. In certain phases of the walking gait, the conditions in (8) are not satisfied leading to dynamic walking. With $\lambda = 0.1$, the stability margin is lesser and the walking speed is higher (approximately 0.128 m/s) than those with $\lambda = 0.15$.

7.2. Effect of step-time (T) on walking performance

With increasing T, the walking process slows down increasing the stability margin and, both f_1 and $f_1^{\max}$ increase. However, $\frac{f_1}{f_1^{\max}}$ does not change, keeping the value

https://doi.org/10.1017/S026357470800475X Published online by Cambridge University Press

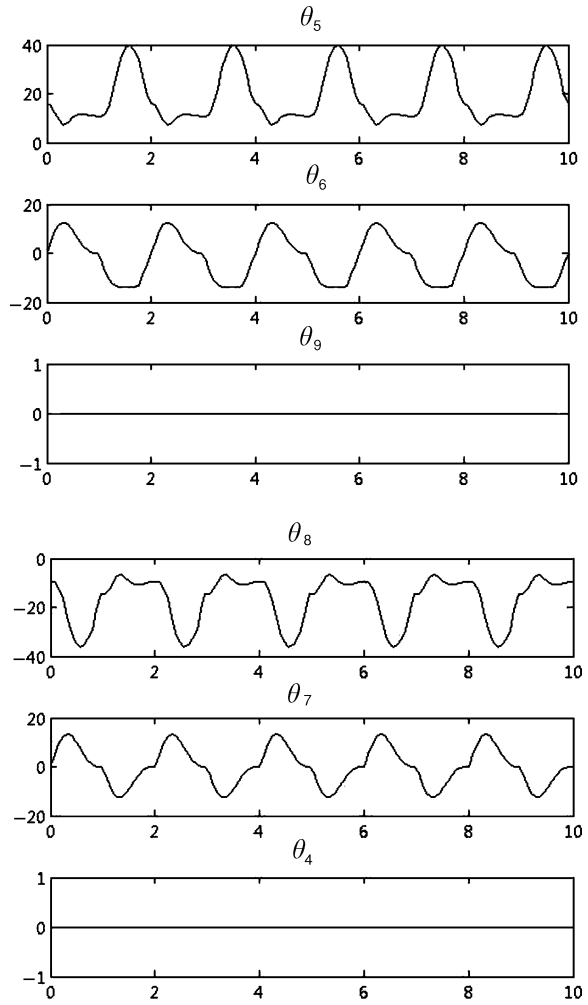

Fig. 10. The walking gait with $\lambda = 0.15$: θ_4, θ_9, θ_5, θ_8, θ_6, θ_7 (time in second vs. angle in degree).

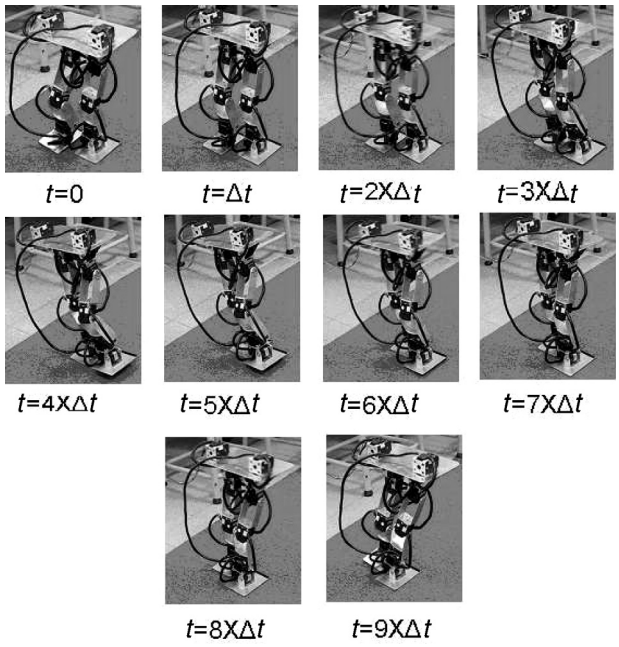

Fig. 11. Biped walking for one step-time with $\lambda = 0.15$.

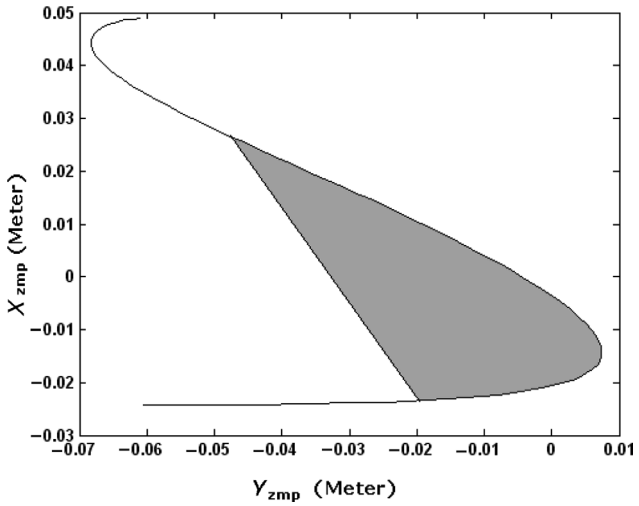

Fig. 12. y_{zmp} vs. x_{zmp} for one step-time with $\lambda = 0.15$.

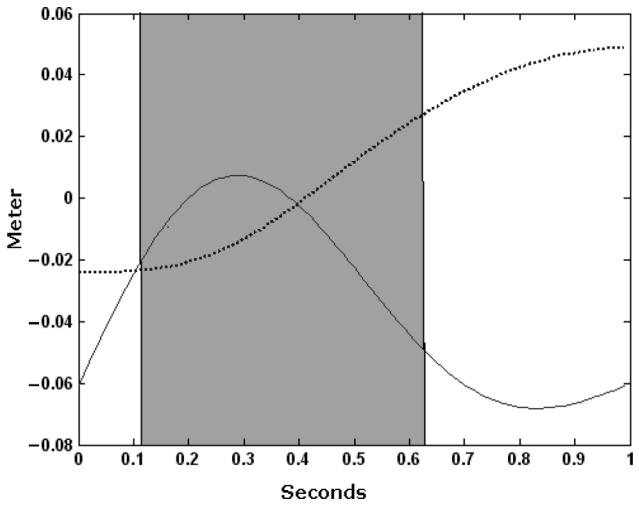

Fig. 13. y_{zmp} and x_{zmp} vs. time for one step-time with $\lambda = 0.15$ (dotted line is x_{zmp} and solid line is y_{zmp}).

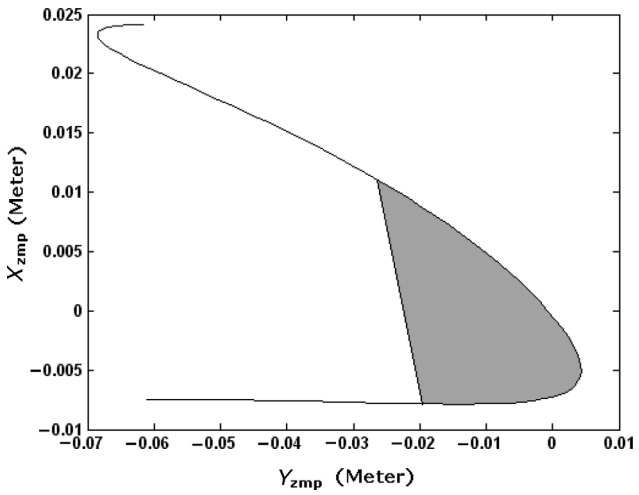

Fig. 14. y_{zmp} vs. x_{zmp} for one step-time with $\lambda = 1.0$.

https://doi.org/10.1017/S026357470800475X Published online by Cambridge University Press

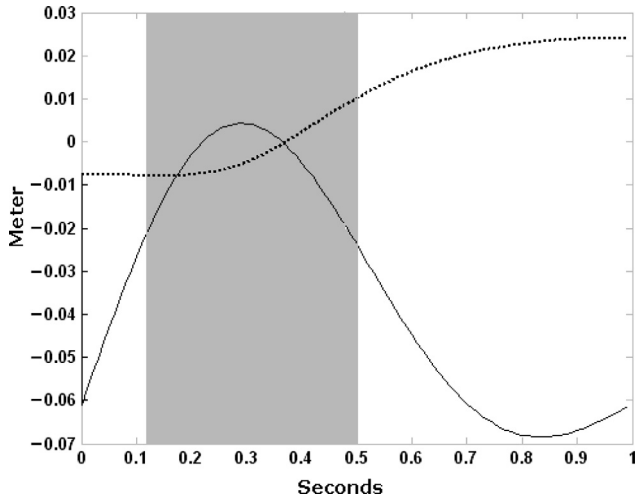

Fig. 15. y_{zmp} and x_{zmp} vs. time for one step-time with $\lambda = 1.0$ (dotted line is x_{zmp} and solid line is y_{zmp}).

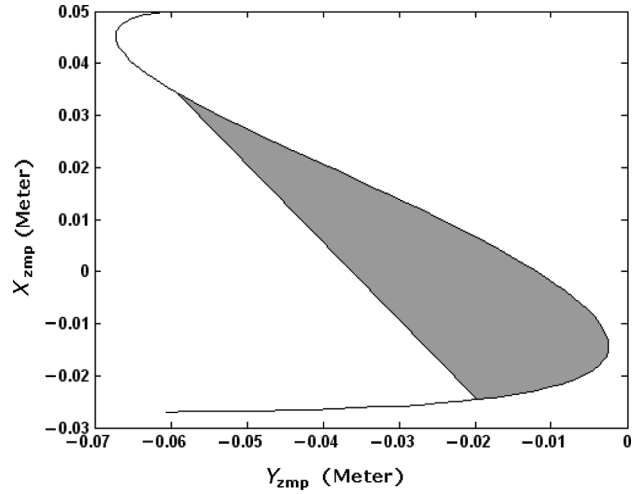

Fig. 16. y_{zmp} vs. x_{zmp} for one step-time with $\lambda = 0.1$.

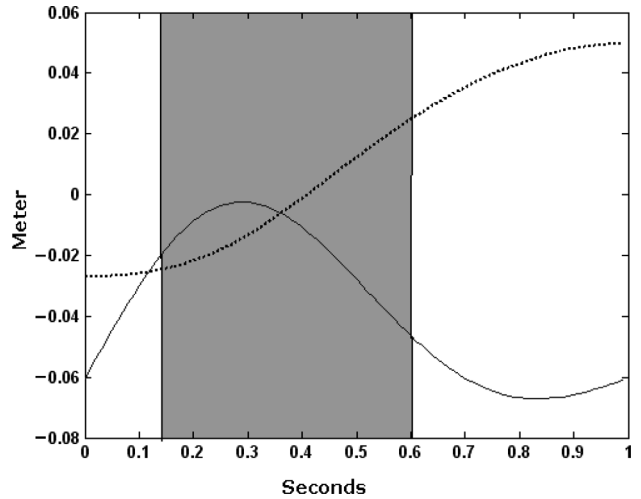

Fig. 17. y_{zmp} and x_{zmp} vs. time for one step-time with $\lambda = 0.1$ (dotted line is x_{zmp} and solid line is y_{zmp}).

Table IV. Walking parameters for different step-time (T).

T	s	n	H	h	$f_1^{\max}$	f
2.0	0.126	0.12	0.014	0.0215	1258.90	0.9596
1.5	0.130	0.11	0.014	0.0220	979.51	0.9612
0.8	0.130	0.12	0.014	0.0200	382.66	0.9585
0.5	0.129	0.11	0.014	0.0210	202.87	0.9645

of f almost unchanged. Table IV shows the optimal walking parameters for $\lambda = 0.15$ with different values of T. The parameters vary nominally with T. With increase in T and constant Δt, sampling frequency ($\frac{T}{\Delta t}$) increases. Sampling frequency decreases when T decreases with constant Δt. If ($\frac{T}{\Delta t}$) is constant, absolute value of T does not have any effect on walking performance. Although, ($\frac{T}{\Delta t}$) can be changed to adjust the walking speed, due to hardware constraints it is not recommended to change ($\frac{T}{\Delta t}$), rather λ or step-length "s" can be adjusted to vary the walking speed.

8. Conclusions

In this work, the walking gait generation of a 12-DOF biped robot is considered. Closed-form solution of the inverse kinematics of the biped is computed. The inverse kinematics is expressed in terms of certain gait parameters. The walking gait is generated based on the parameters. The walking gait is parameterized in terms of four factors, i.e., step-length, bending-height, maximum lifting-height, and maximum frontal-shifting. These walking parameters are then optimized using GA. The optimization is performed as a tradeoff between postural stability and walking speed. The optimal gaits are experimentally realized on a biped robot.

References

1. M. Vukobratović, B. Borovac, D. Surla and D. Stokić, *Biped Locomotion: Dynamics, Stability, Control and Application* (Springer-Verlag, Berlin, 1990).
2. F. Yamasaki, K. Hosoda and M. Asada, "An Energy Consumption Based Control for Humanoid Walking," *IEEE/RS J International Conference on Intelligent Robots and System (IROS)* (Switzerland, Sept. 30–Oct. 5, 2002) Vol. 3, pp. 2473–2477.
3. K. Ono, R. Takahashi, A. Imadu and T. Shimada, "Self-Excitation Control for Biped Walking Mechanism," *IROS* (Japan, Oct. 31–Nov. 5, 2000) Vol. 2, pp. 1143–1148.
4. Kyung-Kon Noh, Jin-Geol Kim and Uk-Youl Huh, "Stability Experiment of a Biped Walking Robot with Inverted Pendulum," *30th IEEE Annual Conference of Industrial Electronics Society* (USA, Nov. 2–6, 2004) Vol. 3, pp. 2475–2479.
5. Hun-ok Lim, Y. Yamamoto and A. Takanishi, "Control to Realize Human-Like Walking of a Biped Humanoid Robot," *IEEE International Conference on Systems, Man, and Cybernetics* (USA, Oct. 8–11, 2000) Vol. 5, pp. 3271–3276.
6. Xiuping Mu and Qiong Wu, "Synthesis of a complete sagittal gait cycle for a five-link biped robot," *Robotica* **21**(05), 581–587 (Oct. 2003).
7. S. Kajita, F. Kanehiro, K. Kaneko, K. Fujiwara, K. Harada, K. Yokoi and H. Hirukawa, "Biped Walking Pattern Generation by Using Preview Control of Zero-Moment Point," *IEEE International Conference on Robotics and Automation (ICRA)* (Taipei, Sept. 14–19, 2003) Vol. 2, pp. 1620–1626.
8. Prahlad Vadakkepat, Dip Goswami and Chia Meng Hwee, "Disturbance rejection by online ZMP compensation," *Robotica* **26**, 9–17, (2007).

https://doi.org/10.1017/S026357470800475X Published online by Cambridge University Press

9. T. Sugihara, Y. Nakamura and H. Inoue, "Real-time Humanoid Motion Generation Through ZMP Manipulation Based on Inverted Pendulum Control," *ICRA* (USA, May 11–15, 2002) Vol. 2, pp. 1404–1409.
10. S. Kitamura, Y. Kurematsu and M. Iwata, "Motion Generation of a Biped Locomotive Robot Using an Inverted Pendulum Model and Neural Networks," *IEEE Conference on Decision and Control* (USA, Dec. 5–7, 1990) Vol. 6, pp. 3308–3312.
11. A. W. Salatian and Y. F. Zheng, "Gait Synthesis for a Biped Robot Climbing Sloping Surfaces Using Neural Networks. II. Dynamic learning," *ICRA* (France, May 12–14, 1992) Vol. 3, pp. 2607–2611.
12. M. Cao and A. Kawamura, "A Design Method of Neural Oscillatory Networks for Generation of Humanoid Biped Walking Patterns," *ICRA* (Belgium, May 16–20, 1998) Vol. 3, pp. 2357–2362.
13. A. Dasgupta and Y. Nakamura, "Making Feasible Walking Motion of Humanoid Robots from Human Motion Capture Data," *ICRA* (USA, May 10–15, 1999) Vol. 2, pp. 1044–1049.
14. Sang-Ho Choi, Young-Ha Choi and Jin-Geol Kim, "Optimal Walking Trajectory Generation for a Biped Robot Using Genetic Algorithm," *IROS* (South Korea, Oct. 17–21, 1999) Vol. 3, pp. 1456–1461.
15. M. Y. Cheng and C. S. Lin, "Genetic Algorithm for Control Design of Biped Locomotion Systems," *IEEE International Conference on Systems, Man and Cybernetics* (Canada, Oct. 22–25, 1995) Vol. 3, pp. 1456–1461.
16. Jung-Shik Kong, Bo-Hee Lee and Jin-Geol Kim, "A Study on the Gait Generation of a Humanoid Robot Using Genetic Algorithm," *SICE 2004 Annual Conference* (Japan, Aug. 4–6, 2004) Vol. 1, pp. 187–191.
17. F. Arakawa and T. Fukuda, "Natural Motion Trajectory Generation of Biped Locomotion Robot Using Genetic Algorithm Through Energy Optimization," *IEEE International Conference on Systems, Man, and Cybernetics* (China, Oct. 14–17, 1996) Vol. 2, pp. 1495–1500.
18. John J. Craig, *Introduction to Robotics: Mechanics and Control*, 2nd ed. (Addison-Wesley Longman Publishing Co., Boston, MA, 1989).
19. Z. Tang, C. Zhou and Z. Sun, "Humanoid Walking Gait Optimization Using GA-Based Neural Network," International Conference on Natural Computation (2) (*ICNC(2)*) (China, 2005) pp. 252–261.
20. Y. Sakagami, R. Watanabec, C. Aoyama, S. Matsunaga and N. Higaki, "The Intelligent ASIMO: System Overview and Integration," *Proceedings of the IEEE/RSJ International Conference on Intelligent Robots and Systems*, Switzerland (2002) pp. 2478–2483.
21. L. Righetti and A. J. Ijspeert, "Programmable Central Pattern Generators: An Application to Biped Locomotion Control," *IEEE International Conference on Robotics and Automation (ICRA06)*, Orlando (2006) pp. 1585–1590.
22. P. Manoonpong, T. Geng, T. Kulvicius, B. Porr and F. Wrgtter, "Adaptive, fast walking in a biped robot under neuronal control and learning," *PLoS Comput Biol* **3**(7), e134 (2007).
23. C. Capaday, "The special nature of human walking and its neural control," *Trends Neurosci* **25**, 370–376 (2002).
24. J. Duysens and V. de Crommert, "Neural control of locomotion. Part 1: The central pattern generator from cats to humans," *Gait Posture* **7**, 131–141 (1998).
25. T. McGeer, "Passive dynamic walking," *Int. J. Rob. Res.* **9**(2), 62–82 (1990).
26. S. H. Collins, A. L. Ruina, R. Tedrake and M. Wisse, "Efficient bipedal robots based on passive-dynamic walkers," *Science* **307**, 1082–1085 (2005).
27. A. J. Ijspeert, A. Crespi, D. Ryczko and J. M. Cabelguen, "From swimming to walking with a salamander robot driven by a spinal cord model," *Science* **315**(5817), 1416–1420 (2007).
28. H. Kimura, Y. Fukuoka and A. H. Cohen, "Adaptive dynamic walking of a quadruped robot on natural ground based on biological concepts," *Int. J. Rob. Res.* **26**(5), 475–490 (2007).
29. P. Manoonpong, F. Pasemann and H. Roth, "Modular reactive neurocontrol for biologically-inspired walking machines," *Int. J. Rob. Res.* **26**(3), 301–331 (2007).
30. R. D. Beer, R. D.Quinn, H. J. Chiel and R. E. Ritzmann, "Biologically inspired approaches to robotics: What can we learn from insects?," *Commun. ACM* **40**(3), 30–38 (1997).
31. T. Geng, B. Porr and F. Wrgtter, "Fast biped walking with a sensor-driven neuronal controller and real-time online learning," *Int. J. Rob. Res.* **25**(3), 243–259 (2006).

Appendix: ZMP computation of the biped

The following expressions are used in the computation of the biped CM in (12) mentioned in Section 6:

$$
\begin{aligned}
\textstyle\sum_i m_i P_{ix} &= -(m_2 + 2m_4)x_1 + m_1 d_2 \cos(\theta_1)\cos(\theta_B) \\
&\quad + m_3 L \cos(\theta_1)\cos(\theta_B) + m_1(x_r + d_2 \cos(\theta_1)\cos(\theta_B)) \\
&\quad + m_3(x_r + L\cos(\theta_1)\cos(\theta_B)), \\
\textstyle\sum_i m_i P_{iy} &= -m_4 y_1 - m_2\left(\frac{w}{2} + y_1\right) - m_4(w + y_1) \\
&\quad + m_1 d_2 \sin(\theta_1)\sin(\theta_B) + m_3 L \sin(\theta_1)\sin(\theta_B) \\
&\quad - m_1(d_2 \sin(\theta_1)\sin(\theta_B) + w) \\
&\quad - m_3(L\sin(\theta_1)\sin(\theta_B) + w), \\
\textstyle\sum_i m_i P_{iz} &= m_3 L\cos(\theta_1)\cos(\theta_B) + m_1 d_2 \cos(\theta_1)\cos(\theta_B) \\
&\quad + (m_2 + 2m_4)P_{6z} + m_1(z_r - z_1 + d_2\cos(\theta_1)\cos(\theta_B)) \\
&\quad + m_3(z_r - z_1 + L\cos(\theta_1)\cos(\theta_B)), \\
\textstyle\sum_i m_i &= 2(m_1 + m_3 + m_4) + m_2. \qquad \text{(A 1)}
\end{aligned}
$$

For the computation of the biped's ZMP in expression (14), the following expressions are used:

$$
\begin{aligned}
\textstyle\sum_i m_i P_{ix}\ddot{P}_{iz} &= m_1 P_{3x}\ddot{P}_{3z} + (m_2 + 2m_4)P_{6x}\ddot{P}_{6z} \\
&\quad + m_1 P_{10x}\ddot{P}_{10z} + m_3 P_{m12x}\ddot{P}_{m12z} + m_3 P_{m0x}\ddot{P}_{m0z}, \\
\textstyle\sum_i m_i P_{iz}\ddot{P}_{ix} &= m_1 P_{3z}\ddot{P}_{3x} + (m_2 + 2m_4)P_{6z}\ddot{P}_{6x} \\
&\quad + m_1 P_{10z}\ddot{P}_{10x} + m_3 P_{m12z}\ddot{P}_{m12x} + m_3 P_{m0z}\ddot{P}_{m0x}, \\
\textstyle\sum_i m_i P_{iy}\ddot{P}_{iz} &= m_1 P_{3y}\ddot{P}_{3z} + m_4 P_{6y}\ddot{P}_{6z} \\
&\quad + m_2\left(P_{6y} - \frac{w}{2}\right)\ddot{P}_{6z} + m_4(P_{6y} - w)\ddot{P}_{6z} \\
&\quad + m_1 P_{10y}\ddot{P}_{10z} + m_3 P_{m12y}\ddot{P}_{m12z} + m_3 P_{m0y}\ddot{P}_{m0z}, \\
\textstyle\sum_i m_i P_{iz}\ddot{P}_{iy} &= m_1 P_{3z}\ddot{P}_{3y} + (m_2 + 2m_4)P_{6z}\ddot{P}_{6y} \\
&\quad + m_1 P_{10z}\ddot{P}_{10y} + m_3 P_{m12z}\ddot{P}_{m12y} + m_3 P_{m0z}\ddot{P}_{m0y}. \qquad \text{(A 2)}
\end{aligned}
$$

In (A 2), the expressions of $P_6(P_{6x}, P_{6y}, P_{6z})$ are given by (6). The expressions of $P_3(P_{3x}, P_{3y}, P_{3z})$, $P_{10}(P_{10x}, P_{10y}, P_{10z})$, $P_{0m}(P_{0mx}, P_{0my}, P_{0mz})$, and $P_{12m}(P_{12mx}, P_{12my}, P_{12mz})$ are computed using (4) and (6). The expressions of the above reference points are given by

$$
\begin{aligned}
P_{3x} &= d_2\cos(\theta_B)\cos(\theta_1), \\
P_{3y} &= d_2\sin(\theta_B)\sin(\theta_1), \\
P_{3z} &= d_2\cos(\theta_1)\cos(\theta_2), \\
P_3 &= [P_{3x}, P_{3y}, P_{3z}]^T. \qquad \text{(A 3)}
\end{aligned}
$$

https://doi.org/10.1017/S026357470800475X Published online by Cambridge University Press

$$
\begin{aligned}
P_{10x} &= x_r - x_1 + d_2 \cos(\theta_D)\cos(\theta_{12}),\\
P_{10y} &= d_2 \sin(\theta_D)\sin(\theta_{12}) - w,\\
P_{10z} &= z_r - z_1 + d_2 \cos(\theta_{11})\cos(\theta_{12}),\\
P_{10} &= [P_{10x}, P_{10y}, P_{10z}]^T. \qquad \text{(A 4)}
\end{aligned}
$$

$$
\begin{aligned}
P_{0mx} &= L \cos(\theta_B)\cos(\theta_1),\\
P_{0my} &= L \sin(\theta_B)\sin(\theta_1),\\
P_{0mz} &= L \cos(\theta_1)\cos(\theta_2),\\
P_{0m} &= [P_{0mx}, P_{0my}, P_{0mz}]^T. \qquad \text{(A 5)}
\end{aligned}
$$

$$
\begin{aligned}
P_{12mx} &= x_r - x_1 + L \cos(\theta_D)\cos(\theta_{12}),\\
P_{12my} &= L \sin(\theta_D)\sin(\theta_{12}) - w,\\
P_{12mz} &= z_r - z_1 + L \cos(\theta_{11})\cos(\theta_{12}),\\
P_{12m} &= [P_{12mx}, P_{12my}, P_{12mz}]^T. \qquad \text{(A 6)}
\end{aligned}
$$

Using (A 1)–(A 6), the closed-form expressions of ZMP are computed with sufficient accuracy without computing system dynamics.

https://doi.org/10.1017/S026357470800475X Published online by Cambridge University Press